An Isolated DC-AC Converter Module Integrating Renewable Energy Source and Energy Storage for Cascaded Inverter

Ritwik Chattopadhyay, Viju Nair. R, Subhashish Bhattacharya
FREEDM Systems Center, Department of Electrical and Computer Engineering
North Carolina State University
Raleigh, North Carolina
rchatto, rvijuna, sbhatta4@ncsu.edu

***Abstract*—Large scale grid integration of renewable energy sources demands the converter systems to work under varying nature of renewable energy source power availability, which can be smoothened and compensated by using an Energy Storage. The large scale integration for renewable energy sources at medium voltage grid level can be accomplished using cascaded modular converter. This paper work focuses on an isolated DC-AC converter module which integrates a renewable energy source, an energy storage and a single phase low frequency AC output port. The converter uses a high frequency transformer with four winding terminals to integrate the renewable energy source, energy storage and the AC output port. The high frequency transformer current control maintains the renewable energy source power output at a fixed dc level without any 2nd harmonic oscillations, while all the 2nd harmonic oscillating component of power is supplied by the energy storage. This paper focuses on the converter working principle, power control and soft-switching ZVS of the converter.**

***Index Terms*—renewable energy source, energy storage, low frequency AC, high frequency transformer, ZVS**

I. Introduction

Large scale grid integration of renewable energy sources (RES) like PV requires an energy storage as a standby support for disturbance free power injection into grid [1]. The integration of Energy Storage(ES) with RES can be carried out by using a separate grid-tied converter, or at a modular level integrating the RES and ES. Integration of ES at modular level provides a better solution from both cost and technical aspects [2]. The evolution of SiC devices have opened the scope for grid integration at medium voltage levels [3], [4]. However, cascaded and modular topologies [5], [6], [8] are still very popular because of their reliability. Since very high voltage SiC devices(10kV or higher) have not been yet commercialized fully for development purpose, using a cascaded converter structure with 1200V/1700V SiC devices provides the designer opportunity to reduce the number of cascaded cells required to match the voltage levels. This paper work proposes an isolated DC-AC converter module, which has DC sources like RES and ES at its input ports and produces a low frequency output AC voltage. The cascaded converter structure and the proposed schematic of the modular building block is shown in Fig. 1. The converter uses a four winding high frequency transformer for power transfer. In Fig. 1, ports 1 and 2 are RES and ES, while ports 3 and 4 produces output dc voltages superimposed with low frequency ac, which are in phase opposition. Hence the difference between port 3 and port 4 dc voltages, cancels the dc voltages and produces a pure low frequency ripple free sinusoidal ac voltage. The power transfer among the different ports are controlled using phase shifts among different winding voltages. The advantage of this converter is it has ZVS soft-switching over certain operating points and does not require high frequency filter unlike two/three level inverters.

II. Converter operation overview and control

The converter of Fig. 1 has a four port high frequency transformer with square wave winding voltages across the four windings. The converter has four H-bridges which produce square wave voltages across their windings, causing power flow among the different ports. In this paper, the winding voltage V_1 is taken as reference voltage, making ϕ_1=0, and the magnetizing inductance Lm of the transformer(equivalent circuit is given in Fig. 2) is considered much high than the leakage inductances. The phasor diagram for the transformer voltages, is given in Fig. 3. The dc side voltages for ports 3 and 4 have dc with varying ac such that $V_{dc3} = V_{dc} + 0.5V\text{msin}(\omega t)$ and $V_{dc4} = V_{dc} - 0.5V_m\text{sin}(\omega t)$, thus $V_{ac} = V_{dc3} - V_{dc4} = V_m\text{sin}(\omega t)$. The converter of Fig. 1 is basically an extension of the three port converter operation as discussed in [7], [9], [11], where the power flow of each port is function of winding voltages and phase angles. In order to control the power flow for different ports of such converter, a decoupling control method is required. A high frequency current control method, which inherits a decoupling within it, has been discussed in [9], [10]. The three port current control of [9] has been extended in this paper, for power control of the four port converter. In this paper, the high frequency currents for ports 1, 3 and 4 are controlled in one switching cycle, which automatically controls the power flow of port 2. From Fig. 2, considering $L_m >> L_1, L_2, L_3, L_4$, the voltage V_m and the slopes m^y for the windings 1, 3 and 4 are given below, where 'y' is the corresponding winding current. Here all the

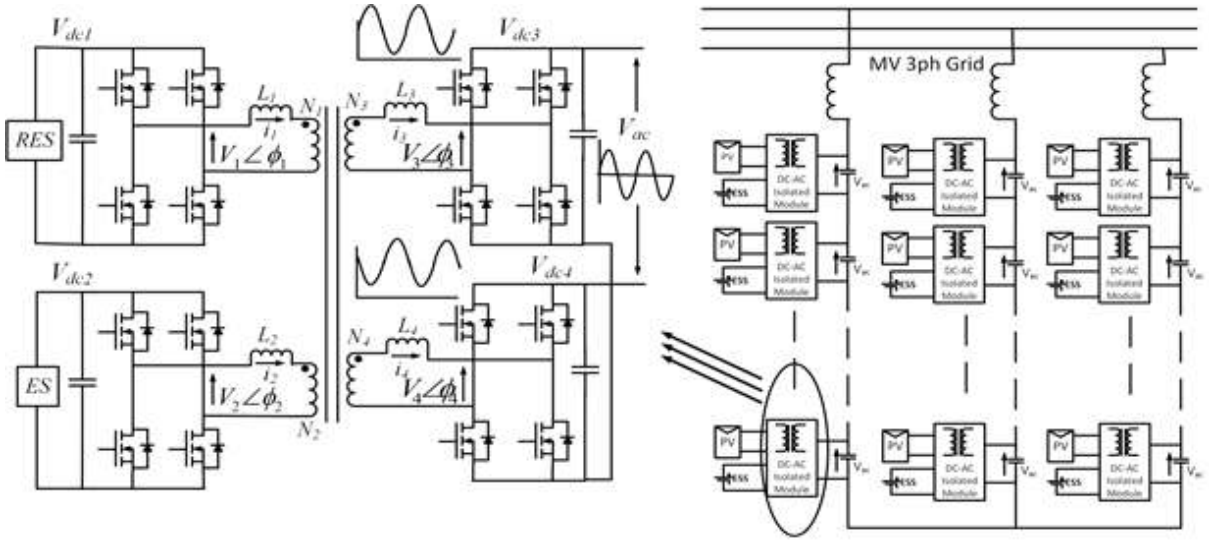

Fig. 1. Isolated DC-AC converter topology for cascaded converter structure .

transformer voltages, currents and inductances are referred to winding 1 for convenience. The current control method for the four port high frequency converter within a single switching cycle control is depicted in Fig. 4. It is assumed the voltages V_{dc3} and V_{dc4} remain constant within one switching cycle, or the switching frequency is much higher than the frequency of the ac output voltage, thus $\omega_s >> \omega$. where $\omega_s=2\pi f_s$, f_s is the switching frequency and K_x^y is the equivalent function of inductances for constant slope interval 'x' for corresponding winding 'y'. The slope for each constant slope interval within a half switching cycle can be expressed as m_x^y. Similar to the method in [9], the currents in the windings 1, 3 and 4 are sampled at mid-point of each half cycle and the phase angles for the next half cycle current values are calculated updated at mid-point of next half. From Fig. 4, the current expressions for different winding currents and the control derivation is given in eqns (6-8). Arranging these equations in matrix form and replacing the slopes m_x^y for each case with expressions from (3-5) using constants 'K_x^y's and winding voltages, the expressions for $\phi_{2(n)}$, $\phi_{3(n)}$, $\phi_{4(n)}$ can be obtained as given in (9). Similarly, the expressions for $\phi_{2(n+1)}$, $\phi_{3(n+1)}$,

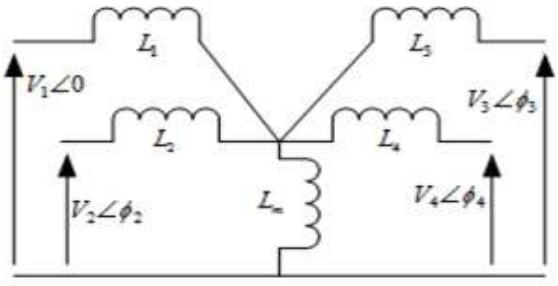

Fig. 2. Equivalent Circuit of Converter (Lm >> L1,L2,L3,L4) .

$$V_m = \frac{V_1L_2L_3L_4 + V_2L_1L_3L_4 + V_3L_1L_2L_4 + V_4L_1L_2L_3}{L^3} \quad (1)$$

$$L^3 = L_2L_3L_4 + L_1L_3L_4 + L_1L_2L_4 + L_1L_2L_3 \quad (2)$$

$$m^1 = \frac{V_1-V_m}{w_sL_1} = (V_1-V_2)K_1^1 + (V_1-V_3)K_2^1 + (V_1-V_4)K_3^1 \quad (3)$$

$$m^3 = \frac{V_m-V_3}{w_sL_3} = (V_1-V_3)K_1^3 + (V_2-V_3)K_2^3 + (V_4-V_3)K_3^3 \quad (4)$$

$$m^4 = \frac{V_m-V_4}{w_sL_4} = (V_1-V_4)K_1^4 + (V_2-V_4)K_2^4 + (V_3-V_4)K_3^4 \quad (5)$$

$\phi_{4(n+1)}$ can be expressed as shown in (10). Clearly, the inverse matrix in equations (9) and (10) can be pre-calculated, and the other matrices can be evaluated from sensed dc voltages and winding currents. Similar as explained in [9], the equations for transformer current control derived here, is for the situation of Fig. 3 and Fig. 4, but the same set of equations apply to other cases as well. The solution set of equations (9) and (10) are generic solutions for the current control of four port high frequency transformer with decoupling. The ac output voltage is generated from the difference of voltages V_{dc3} and V_{dc4}. The overall control loop schematic is shown in figure 5. The RES of port 1 has a dc current reference of $I_{1,dc\text{-}ref}$ and the voltages V_{dc3} and V_{dc4} have the references $V_{dc3\text{-}ref} = V_{dc} + 0.5\sin(\omega t)$ and $V_{dc4\text{-}ref} = V_{dc} - 0.5\sin(\omega t)$. The errors for I_{1dc}, V_{dc3} and V_{dc4} are fed to the controllers which generates the references for the transformer winding currents i_1, i_3 and i_4. The single phase ac output voltage generates a second harmonic power oscillation, which is reflected on the ES port. The dc current control loop of Fig. 8 maintains the RES power at a steady dc value, while all the second harmonic power oscillation is supplied from the Energy Storage(ES) port. The high frequency transformer current control described above controls the transformer current within one switching cycle for the given transformer current references i_{1_ref}, i_{3_ref}, i_{4_ref}. Hence the control loops for $I_{1,dc}$, V_{dc3} and V_{dc4} can have higher

$$i_{1ref}=i_{1(n)}=i_{1(n-2)} + m_4^1(\pi/2) - m_1^1\phi_{2(n-1)} - m_2^1(\phi_{3(n-1)} - \phi_{2(n-1)}) - m_3^1(\phi_{4(n-1)} - \phi_{3(n-1)}) - m_4^1(\pi/2 - \phi_{4(n-1)})$$

$$+ m_1^1\phi_{2(n)} + m_2^1(\phi_{3(n)} - \phi_{2(n)}) - m_3^1(\phi_{4(n)} - \phi_{3(n)}) + m_4^1(\pi/2 - \phi_{4(n)}) \quad (6)$$

$$i_{3ref}=i_{3(n)}=i_{3(n-2)} + m_4^3(\pi/2) - m_1^3\phi_{2(n-1)} - m_2^3(\phi_{3(n-1)} - \phi_{2(n-1)}) - m_3^3(\phi_{4(n-1)} - \phi_{3(n-1)}) - m_4^3(\pi/2 - \phi_{4(n-1)})$$

$$+m_1^3\phi_{2(n)} + m_2^3(\phi_{3(n)} - \phi_{2(n)}) - m_3^3(\phi_{4(n)} - \phi_{3(n)}) + m_4^3(\pi/2 - \phi_{4(n)}) \quad (7)$$

$$i_{4ref}=i_{4(n)}=i_{4(n-2)} + m_4^4(\pi/2) - m_1^4\phi_{2(n-1)} - m_2^4(\phi_{3(n-1)} - \phi_{2(n-1)}) - m_3^4(\phi_{4(n-1)} - \phi_{3(n-1)}) - m_4^4(\pi/2 - \phi_{4(n-1)})$$

$$+m_1^4\phi_{2(n)} + m_2^4(\phi_{3(n)} - \phi_{2(n)}) - m_3^4(\phi_{4(n)} - \phi_{3(n)}) + m_4^4(\pi/2 - \phi_{4(n)}) \quad (8)$$

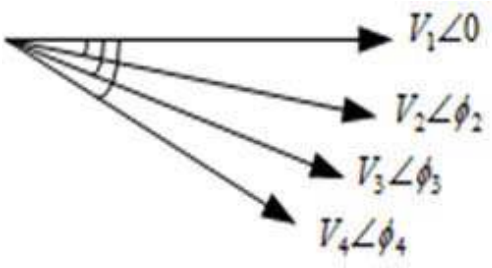

Fig. 3. Phasor Diagram for Four Winding Voltages.

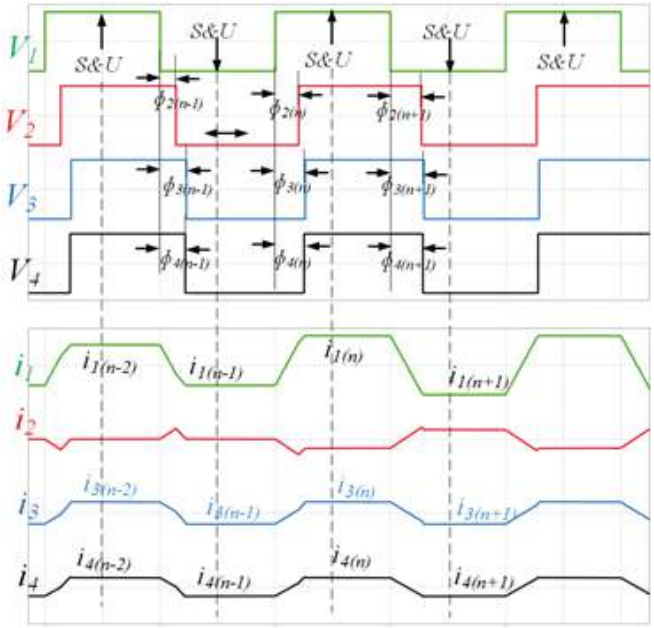

Fig. 4. Current Control Waveform for the 4-port Converter.

bandwidth, around 1/5th of switching frequency and provide fast response for disturbances. The dc voltage control loop has a combined PI and resonant controller tuned at output ac voltage frequency, since the dc signals V_{dc3} and V_{dc4} have ac voltages superimposed on dc voltage. The PI controller controls the dc changes and the resonant controller controls the ac changes.

III. Simulation Study for DC-AC Converter

The simulation study for the isolated DC-AC converter of Fig. 1 is performed based on an approximate 10kW system. The system under study has RES and ES voltages of 800V each and the ac voltage magnitude is decided based on converter control. In this paper, the dc voltage ratings of all the four ports are considered equal to 800V, i.e. $V_{dc1} = V_{dc2} = V_{dc} = 800V$. The ac peak voltages for ports 3 and 4 are considered to be half of the constant dc voltages, i.e. $0.5V_m = 0.5V_{dc} = 400V$. The voltages V_{dc3} and V_{dc4} therefore have positive and negative peak values of $V_{dc3\_peak1} = 1200V$ and $V_{dc3\_peak2} = 400V$. The simulation platform used in PLECS Simulator for power electronic simulation. A preliminary transformer design is carried out using 3C90 Ferrite material for 50kHz operation and the leakage inductances are estimated from Ansys Maxwell FEA simulation of the transformer. The flux density for V_{dc}=800V is taken at 0.2T so that for peak of 1200V, the maximum possible flux density is 0.3T, which is less than ferrite saturation limit. Figure 6 shows the FEA model for the transformer. The leakage inductances for the transformer is calculated from L matrix obtained from the FEA simulation. The leakage between any two windings is given as $L_{ij}=L_i+L_j=L_{ii}-M^2/L_{jj}$. From all the combinations of 'i' and 'j', the individual leakage inductances of the circuit model of Fig. 2 is evaluated. Using the individual leakage inductance values, the inductance matrices are pre-calculated. The simulation model for the high frequency transformer is created using PLECS magnetic circuits to verify the flux nature in the transformer core. Simulations for the single stage DC-AC converter of Fig. 1 is shown in Figs 6-10. Figure 7 shows the dc currents and voltages along with output ac voltage and load current for R-L load. It can be seen that as the RES input dc current $I_{1,dc}$ is changed near t=0.08 sec, the

$$\begin{bmatrix}\phi_{2(n)}\\ \phi_{3(n)}\\ \phi_{4(n)}\end{bmatrix} = \begin{bmatrix}K_1^{\,1} & K_2^{\,1} & K_3^{\,1}\\ -K_2^{\,3} & K_{sum}^{\,3} & -K_3^{\,3}\\ -K_2^{\,4} & -K_3^{\,4} & K_{sum}^{\,4}\end{bmatrix}^{-1} \begin{bmatrix}i_{1ref}-i_{1(n-2)}\\ i_{3ref}-i_{3(n-2)}\\ i_{4ref}-i_{4(n-2)}\end{bmatrix} \begin{bmatrix}0.5/V_{dc2} & 0.5/V_{dc3} & 0.5/V_{dc4}\\ 0.5/V_{dc2} & 0.5/V_{dc3} & 0.5/V_{dc4}\\ 0.5/V_{dc2} & 0.5/V_{dc3} & 0.5/V_{dc4}\end{bmatrix} + \begin{bmatrix}\phi_{2(n-1)}\\ \phi_{3(n-1)}\\ \phi_{4(n-1)}\end{bmatrix} \quad (9)$$

$$\begin{bmatrix}\phi_{2(n+1)}\\ \phi_{3(n+1)}\\ \phi_{4(n+1)}\end{bmatrix} = \begin{bmatrix}K_1^{\,1} & K_2^{\,1} & K_3^{\,1}\\ -K_2^{\,3} & K_{sum}^{\,3} & -K_3^{\,3}\\ -K_2^{\,4} & -K_3^{\,4} & K_{sum}^{\,4}\end{bmatrix}^{-1} \begin{bmatrix}-i_{1ref}-i_{1(n-1)}\\ -i_{3ref}-i_{3(n-1)}\\ -i_{4ref}-i_{4(n-1)}\end{bmatrix} \begin{bmatrix}0.5/V_{dc2} & 0.5/V_{dc3} & 0.5/V_{dc4}\\ 0.5/V_{dc2} & 0.5/V_{dc3} & 0.5/V_{dc4}\\ 0.5/V_{dc2} & 0.5/V_{dc3} & 0.5/V_{dc4}\end{bmatrix} + \begin{bmatrix}\phi_{2(n)}\\ \phi_{3(n)}\\ \phi_{4(n)}\end{bmatrix} \quad (10)$$

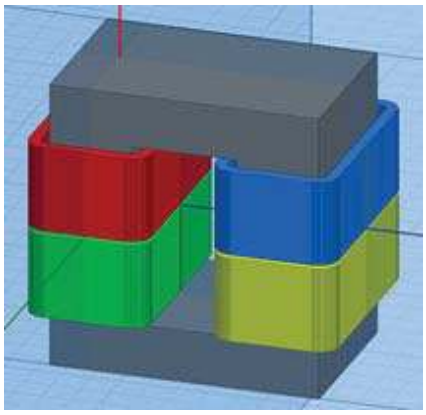

Fig. 5. FEA model of four winding transformer.

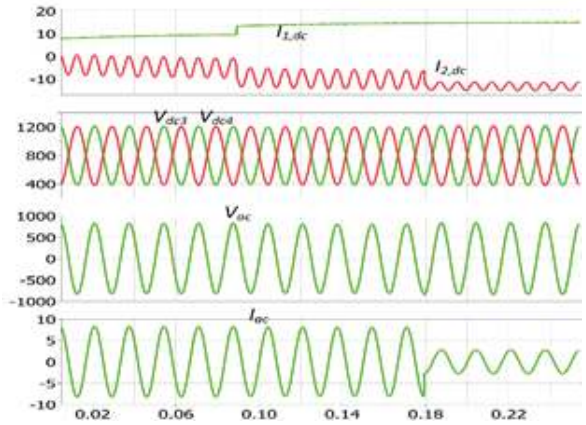

Fig. 6. Input currents and output voltages.

ES dc current $I_{2,dc}$ changes and takes in the extra power and a load change occurs near t=0.18 sec. The ac output voltage remains undisturbed due to these changes. The dc current $I_{1,dc}$ is maintained at pure dc by the current controller and all the 120Hz oscillations for single phase power is supplied from ES, thus utilizing the RES at its full capacity. Figure 8 shows the transformer waveforms over two 60Hz cycles, it can be seen that peak of the transformer voltages V_3 and V_4 oscillate at 60Hz, while the peak of winding currents i_2, i_3 and i_4 oscillate at 120Hz. The winding voltages and currents are expanded near the positive peak of V_{dc3} in Fig. 9 and near the negative peak of V_{dc3} in Fig. 10 It can be observed that the H-bridge converters for ports 1, 2, 3 has ZVS switching(lagging outgoing current and leading input current) in Fig. 9 while H-bridge converters for ports 1, 2, 4 has ZVS switching(lagging outgoing current and leading input current) in Fig. 10. The H-bridges for ports 3 and 4 have loss of ZVS switching over some of the operating range.

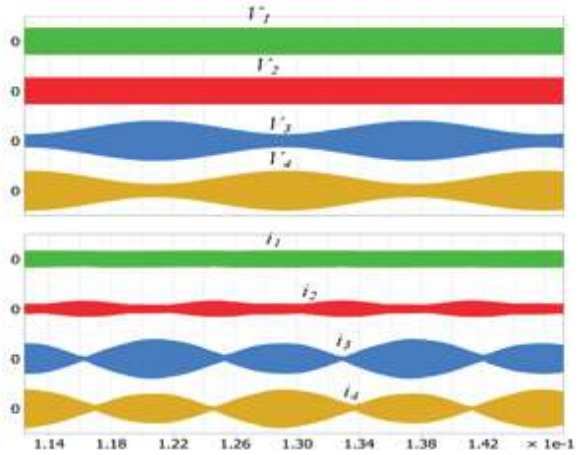

Fig. 7. Transformer waveforms with 120Hz oscillations.

Natural zero voltage switching turn-on or ZVS turn-on operation for high frequency switching based DAB converters is a significant advantage over other hardswitched converters. For converters using Mosfet devices, ZVS turn-on is important for higher switching frequency as most of the Mosfet switching loss takes place during hard turn-on. However, with the advent of SiC Mosfet devices, hard turn-on operation of converter can be allowed to some extent provided converter efficiency target is met. For the converter of Fig. 1 with the phase shift control technique, the ideal ZVS scenarios is discussed here. For a switching device like a Mosfet or IGBT, natural ZVS turn-on takes place when prior to the turn on of a device, the current is flowing in the circuit in an opposite direction to the positive channel conduction direction of the device [12]. In other words, before the device turns on, the circuit current

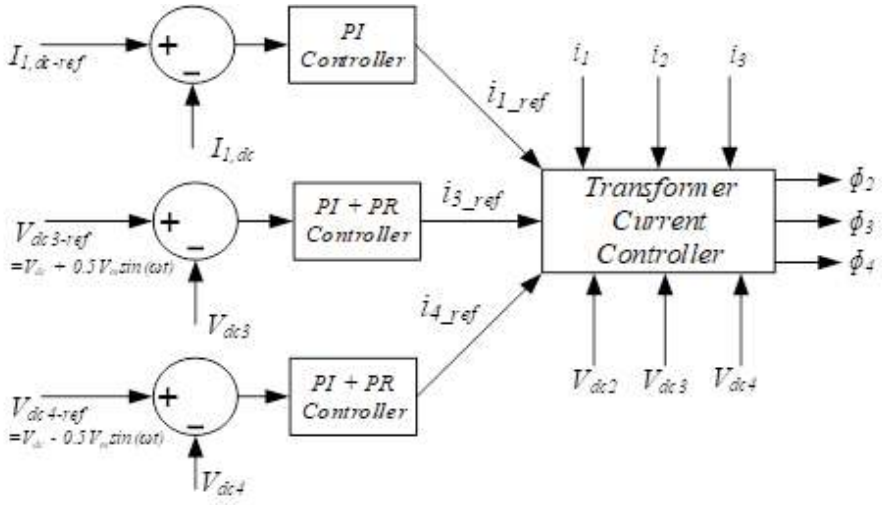

Fig. 8. Power and voltage control loop for isolated DC-AC converter with transformer current control.

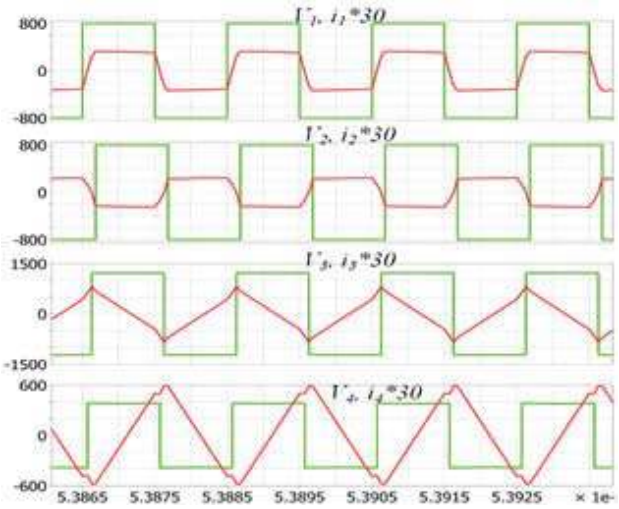

Fig. 9. Transformer waveforms during positive peak of Vac.

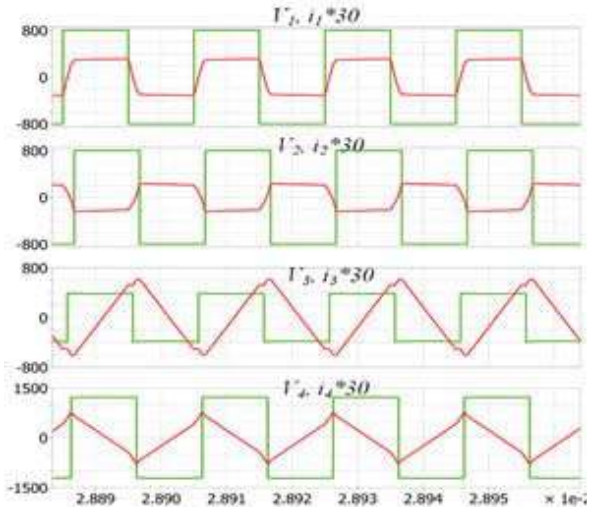

Fig. 10. Transformer waveforms during negative peak of Vac.

flows through the anti-parallel diode when the positive gate signal to the device is applied. Fig. 11 shows the device voltage and current waveforms of one of the switches from each of the four converters in the different sections of V_{ac} from (a) to (d). Fig. 11(a) shows the device voltage and currents during the positive zero crossing of the V_{ac}. It can be seen that all the devices shown in traces 2-5 undergo ZVS, since the voltage drop across the device is zero when the current is transfered to the channel from the anti parallel diode. In Fig. 11(b) during the positive peak of V_{ac}, the switch in port 4 (trace 5) does not undergo ZVS since there is significant voltage when the current is shifted to the device. The same explanation holds for trace 5 in Fig. 11(c) during the descending of V_{ac}. The switch in port 3 also looses ZVS around the negative peak of V_{ac} for the same reason as shown in Fig. 11(d).

IV. Conclusion

The converter of Fig. 1 effectively generates ripple free sinusoidal single phase ac voltage with the proposed control method, which is stiffly able to maintain the output voltage under disturbance scenarios. The working principle, power control and soft switching ZVS is discussed. For large scale grid integration, this converter can be stacked together in all the 3 phases and fed to a 3-phase medium voltage grid. The use of SiC mosfets enables the lower number of cascaded cells to match the voltage levels. The preliminary simulation study conducted in this paper ensures that this converter with a four winding high frequency transformer, integrating PV and ES at the modular level, is a viable scheme for large scale grid integration.

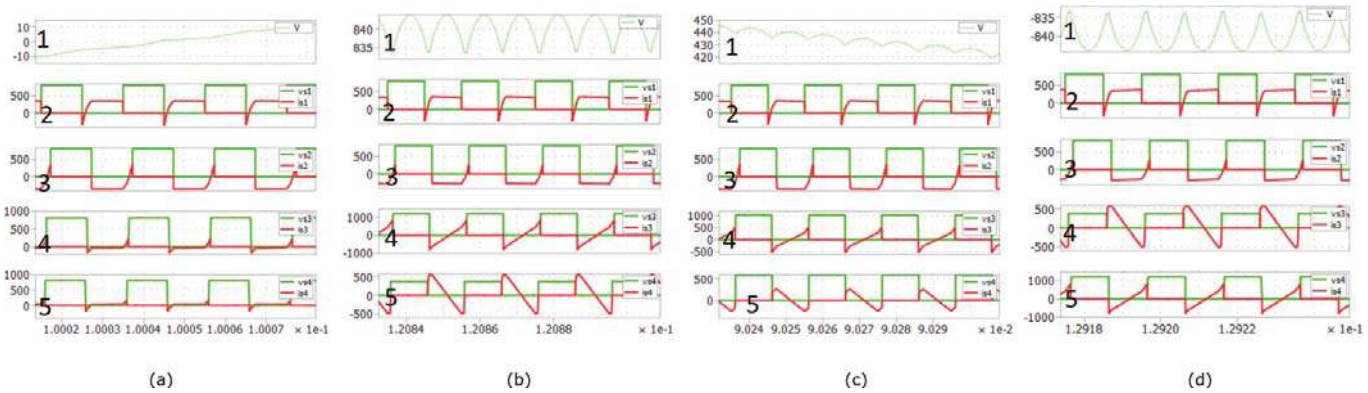

Fig. 11. Voltage and current waveforms of the switches in the four H-bridge converters to analyze ZVS in the different sections of V_{ac}.

REFERENCES

[1] Hu Xie, Shu Zheng, Ming Ni, Microgrid Development in China: A method for renewable energy and energy storage capacity configuration in a megawatt-level isolated microgrid., IEEE Electrification Magazine., vol. 5, Issue. 2, pp. 28-35, 2017.

[2] Paul Denholm, Josh Eichman, Robert Margolis, Evaluating the Technical and Economic Performance of PV Plus Storage Power Plants, Technical Report, National Renewable Energy Laboratory, Aug. 2017.

[3] J. Thoma, D. Kranzer, Demonstration of a Medium Voltage Converter with High Voltage SiC Devices and Future Fields of Application, Proceedings of PCIM Europe 2015, International Exhibition and Conference for Power Electronics, Intelligent Motion, Renewable Energy and Energy Management, pp. 1-8.

[4] S. Hazra et al., "High Switching Performance of 1700-V, 50-A SiC Power MOSFET Over Si IGBT/BiMOSFET for Advanced Power Conversion Applications," in IEEE Transactions on Power Electronics, vol. 31, no. 7, pp. 4742-4754, July 2016.

[5] C. D. Townsend, Y. Yu, G. Konstantinou, V. G. Agelidis, Cascaded H-Bridge Multilevel PV Topology for Alleviation of Per-Phase Power Imbalances and Reduction of Second Harmonic Voltage Ripple, IEEE Trans. Power Electron., vol. 31, Issue. 8, pp. 55745586, 2016.

[6] Yan Zhou, Hui Li, Analysis and Suppression of Leakage Current in Cascaded-Multilevel-Inverter-Based PV Systems, IEEE Trans. Power Elect., vol. 29, Issue. 10, pp. 52655277, 2014.

[7] C. Zhao, S. D. Round, J. W. Kolar, An Isolated Three-Port Bidirectional DC-DC Converter With Decoupled Power Flow Management, IEEE Trans. Power Elect., vol. 23, Issue. 5, pp. 24432453, 2008.

[8] Viju Nair. R, Arun Rahul, S. Kaarthik, A. Kshirsagar and K. Gopakumar, "Generation of Higher Number of Voltage Levels by Stacking Inverters of Lower Multilevel Structures With Low Voltage Devices for Drives," in IEEE Transactions on Power Electronics, vol. 32, no. 1, pp. 52-59, Jan. 2017.

[9] R. Chattopadhyay, S. Acharya, G. Gohil, S. Bhattacharya, One switching cycle current control strategy for triple active bridge phase-shifted DC-DC converter, IEEE Industry Applications Society Annual Meeting, pp. 18, 2017.

[10] R. Chattopadhyay and S. Bhattacharya, "Decoupled power flow using phase shift control and ZVS cases for a three limb high frequency transformer based three-port DAB integrating PV and energy storage," 2016 IEEE Industry Applications Society Annual Meeting, Portland, OR, 2016, pp. 1-8.

[11] Chuanhong Zhao and J. W. Kolar, "A novel three-phase three-port UPS employing a single high-frequency isolation transformer," 2004 IEEE 35th Annual Power Electronics Specialists Conference, 2004, pp. 4135-4141 Vol.6.

[12] R. Chattopadhyay and S. Bhattacharya, "ZVS analysis and power flow control for three limb transformer enabled SiC Mosfet based three port DAB integrating PV and Energy Storage(ES)," 2016 IEEE Energy Conversion Congress and Exposition (ECCE), Milwaukee, WI, 2016, pp. 1-8.